Controlled Fabrication of High-Quality Carbon Nanoscrolls from Monolayer Graphene

ARTICLE *in* NANO LETTERS · JULY 2009

Impact Factor: 13.59 · DOI: 10.1021/nl900677y · Source: PubMed

NANO LETTERS

2009
Vol. 9, No. 7
2565-2570

Controlled Fabrication of High-Quality Carbon Nanoscrolls from Monolayer Graphene

Xu Xie,† Long Ju,† Xiaofeng Feng, Yinghui Sun, Ruifeng Zhou, Kai Liu, Shoushan Fan, Qunqing Li,* and Kaili Jiang*

Department of Physics and Tsinghua-Foxconn Nanotechnology Research Center, Tsinghua University, Beijing 100084, China

Received March 3, 2009; Revised Manuscript Received May 13, 2009

ABSTRACT

We report a simple and effective way of fabricating high-quality carbon nanoscrolls (CNSs), using isopropyl alcohol solution to roll up monolayer graphene predefined on SiO_2/Si substrates. Transmission electron microscopy studies reveal that the CNS has a tube-like structure with a hollow core surrounded by graphene walls 0.35 nm apart. Raman spectroscopy studies show that the CNS is free of significant defects, and the electronic structure and phonon dispersion are slightly different from those of two-dimensional graphene. Finally, the CNS-based device is fabricated, directly on the SiO_2/Si substrate. Electrical-transport measurements show that its resistance is weakly gate-dependent but strongly temperature-dependent. In addition, the CNS can sustain a high current density up to 5×10^7 A/cm^2, indicating that it is a good candidate for microcircuit interconnects. The controlled fabrication of high-quality CNSs may open up new opportunities for both fundamental and applied research of CNSs.

Figure 1. Structural representations of graphene, MWCNT, and CNS.

Over the past several years, carbon nanomaterials such as carbon nanotubes (CNTs)[1] and graphene[2] have been actively explored due to their ideal one-dimensional (1D) and two-dimensional (2D) structures and their excellent properties, which suggest promising applications in many fields. Recently, another interesting carbon nanomaterial, called carbon nanoscroll (CNS), has emerged. It is a spirally wrapped 2D graphene sheet with a 1D tubular structure resembling that of a multiwalled carbon nanotube (MWCNT) (Figure 1). CNS is expected to inherit some excellent properties from both graphene and CNTs, such as high carrier mobility and high mechanical strength. On the other hand, such a hybrid structure should also possess some properties quite distinct from those of graphene and CNTs. For example, the electronic transport of CNS should be affected by the $\pi-\pi$ interaction between the inner and outer surfaces of wrapped graphene as compared with a flat sheet. Also, the electric current flows within a single scrolled graphene layer rather than through several coaxially nested graphene cylinders as in the case of MWCNTs. Theoretical calculations indeed predict some unusual electronic[3] and optical properties[4] of CNS because of its unique topology. In addition, the interlayer spaces of CNS can be easy intercalated because it is not a closed topological structure. This is in sharp contrast to MWCNT, the rigid graphene cylinders of which will resist lattice expansion due to intercalation. Therefore, CNS facilitates chemical doping[5] and hydrogen storage[6,7] and could be utilized in super capacitors and batteries.[5] Since the diameter of CNS can be easily expanded by charge injection or intercalation, it could also be used as a nanoactuator in nanomechanical devices.[5,8] Although there are abundant theoretical predictions, few experimental investigations on CNS have been reported. For instance, up to now its electronic structure remains experimentally untouched, either through optical methods or transport measurements. The challenges are how to fabricate high-purity and high-quality CNSs and integrate them into devices.

* To whom correspondence should be addressed. E-mail: (K.J.) JiangKL@tsinghua.edu.cn; (Q.L.) QunqLi@tsinghua.edu.cn. Tel.: +86 10 62796017; +86 10 62796019. Fax: +86 10 62792457.
† These authors contributed equally to this work.

10.1021/nl900677y CCC: $40.75
Published on Web 06/05/2009

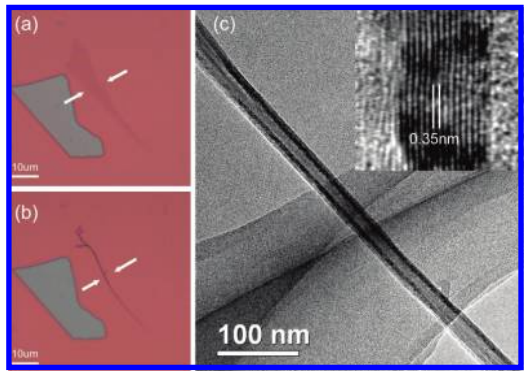

Figure 2. Optical microscope images of the original (a) and scrolled (b) graphene monolayer on the SiO_2 substrate. (c) TEM image of a fabricated CNS. The inset is a higher magnification image of part of the CNS, showing that the distance between adjacent graphene layers is about 0.35 nm.

Previously, several methods have been developed for fabricating CNS, including arc-discharge,[9] high-energy ball milling of graphite,[10] and the chemical route.[11−13] While CNSs may exist in the products of arc-discharge and high-energy ball milling, these fabrication processes are difficult to control and the products are always mixed with abundant graphite and amorphous carbon. It is almost impossible to isolate CNSs from this complex mixture. In the chemical route, graphite is first intercalated and separated into thin layers. Upon sonication, some of the exfoliated graphite sheets curl into scrolls. The advantage of this route is its higher yield of CNSs, but the drawbacks are that they have poor morphologies and are scrolled from an undefined number of graphene layers (one, two, or several). In addition, the chemical process may induce unexpected defects in the CNS, which may degrade its quality. The experimental difficulties in fabrication, isolation, and device integration of high-quality CNS impede the investigation of its physical properties and further applications.

Recently, high-purity and high-quality monolayer graphene can be easily fabricated on SiO_2/Si substrates by a simple mechanical exfoliation method.[14,15] If the graphene monolayers can be rolled up in situ, CNSs with predefined layers of graphene can be directly fabricated without extra isolation, thus facilitating the fabrication of CNS-based devices for investigating its physical properties and future applications. On the basis of molecular dynamic simulations, Yu and Liu have suggested that graphene nanoribbons could be rolled up through adsorption of gas atoms.[16] The feasibility of this method has recently been experimentally verified.[17] Here we report another simpler but more efficient method for in situ fabrication of high-quality CNSs and their direct incorporation into devices. On the basis of this method, their physical properties, such as Raman spectra and electronic transport, have been successfully investigated.

Graphene were first extracted by mechanical exfoliation[15] of natural graphite on degenerately doped Si wafer covered with 285 nm SiO_2. After selecting suitable graphene samples under an optical microscope,[18] we identified their numbers of layers according to their Raman spectra[19] (Supporting Information, Part 1). Usually, monolayer graphene were located (Figure 2a) for use. We then immersed the chip into a Petri dish filled with isopropyl alcohol (IPA) for about 5 min. Afterward, the chip was picked up and dried with nitrogen. Surprisingly, we found that the graphene had turned from a 2D sheet to a 1D fiber-like structure (Figure 2b) after the above procedures. To clarify this fiber-like structure, we transferred it to a transmission electron microscope (TEM) grid for TEM study using a nanoprobe system (Supporting Information, Part 2). The TEM image (Figure 2c) shows that it possesses a tube-like structure with a hollow core surrounded by thick walls consisting of graphene layers. In addition, the enlarged high-resolution TEM image (Figure 2c inset) of the walls shows the graphene layers are uniformly and compactly stacked. The distance between adjacent graphene layers is about 0.35 nm, which is consistent with that of graphite and MWCNT,[1] indicating that there is no contamination between these stacked graphene layers. These TEM results imply that the fabricated 1D structure is a CNS rolled up from a graphene monolayer.

To clarify how the scroll is formed, we then monitored and recorded the entire process using a CCD camera on an optical-microscope (Supporting Information, Part 6). After a droplet of IPA solution (IPA/water $\sim$ 1:3) was placed on the graphene monolayer, one of its straight edges started to roll up. However, the rolling process stopped before the IPA solution evaporated, leaving large part of the graphene remaining flat. Then another droplet of pure IPA solution was added, the scrolling process continued until the whole graphene sheet was rolled up into a CNS. It was found that not every graphene monolayer could be rolled up. Some remained unchanged in the IPA solution, especially those that had irregular shapes or were heavily contaminated. From these observations, we can infer that it is the IPA that helps to roll up the graphene, and this process is sensitive to both contamination and the shape of the graphene.

The CNS formation process can be further understood by the aid of the following four proposed steps (Figure 3). The first step occurred after the chip with graphene was immersed into IPA solution, in which case the upper and lower surfaces of the graphene were in contact with IPA and SiO_2 respectively, resulting in a surface strain in the graphene. This surface strain served as one of the driving forces to bend the graphene sheet.[16,20−23] In the second step, the edges of the graphene were lifted up from the substrate by the surface strain. Then IPA molecules entered into the space between graphene and the substrate, which also facilitated the detachment of the graphene. In the third step, the detached parts of the graphene curved due to perturbations in the solution environment. Once the free end touched another part of the graphene by chance, the $\pi-\pi$ interaction of the overlapped parts decreased the total free energy of graphene,[5] even though the curvature energy increased due to bending. In this case, the scrolling process proceeded continuously in the final step (Step 4), that is, the graphene became detached from the substrate and rolled up bit by bit until a CNS was formed with a decrease in total free energy. The analysis described above is simple and qualitative. To

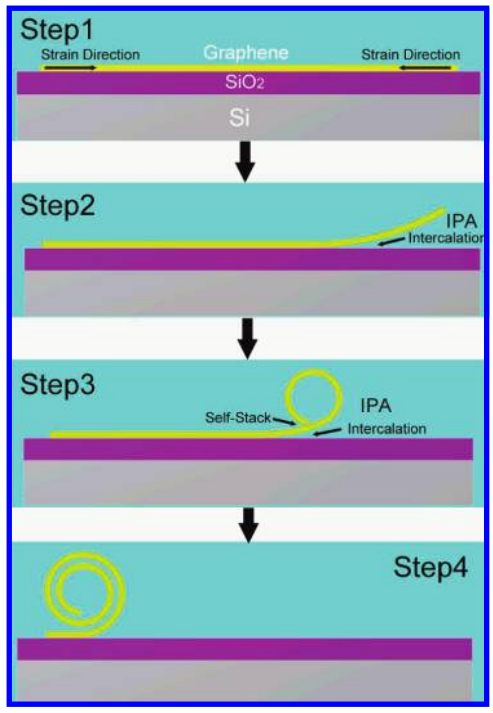

Figure 3. Schematic representation of the formation of CNS. Step1: surface strain is induced in graphene after it is immersed in IPA solution. Step2: the edge of graphene is lifted up with the help of the surface strain and the intercalation of IPA solution. Step3: the initial bending of the graphene is energetically unfavorable and might be caused by perturbations. Once the graphene gets self-stacked, the scrolling process will be easier. Step4: the graphene continued to roll up until a CNS is formed.

explain the mechanism quantitatively, the surface and interfacial energy change during the scrolling process must be calculated.

On the basis of the above analysis, we optimized the scrolling process in the following three aspects. First, the scrolling speed was adjusted by using IPA with different concentrations. We found that pure IPA was too harsh for scrolling, with the products usually consisting of folded graphene (Figure 4a) rather than CNSs. By diluting the IPA solution with water, we successfully slowed down the scrolling process. This is crucial for the formation of CNS. Otherwise if the graphene detaches from the substrate more quickly than it scrolls, direct folding might occur, giving rise to a sophisticated structure. Second, the shape of graphene was preselected to facilitate scrolling. Graphene sheets with irregular shapes were likely to be pinned down during the scrolling process, leaving an unfinished CNS (Figure 4b). On the other hand, a long smooth edge was beneficial for scrolling and the sheets tended to scroll along this edge. Third, the graphene was protected from contamination. We noticed that heavily contaminated graphene was hard to scroll. The scrolling process is sensitive to the contamination, which could modify the surface and edges of the graphene. Therefore, in order to fabricate high-quality CNS, the graphene needs to be carefully protected. After these optimizing procedures, well-stacked CNSs resembling MWCNTs could be obtained (Figure 4c,d).

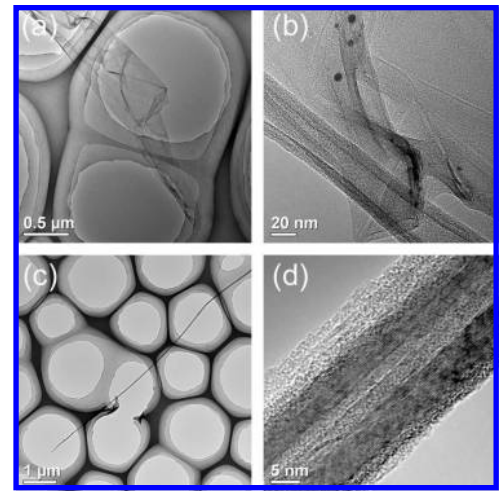

Figure 4. (a) TEM image of a folded graphene monolayer resulting from a harsh fabrication process. (b) TEM image of an unfinished CNS. (c) TEM image of a well-stacked CNS. (d) HRTEM image of part of the CNS shown in (c).

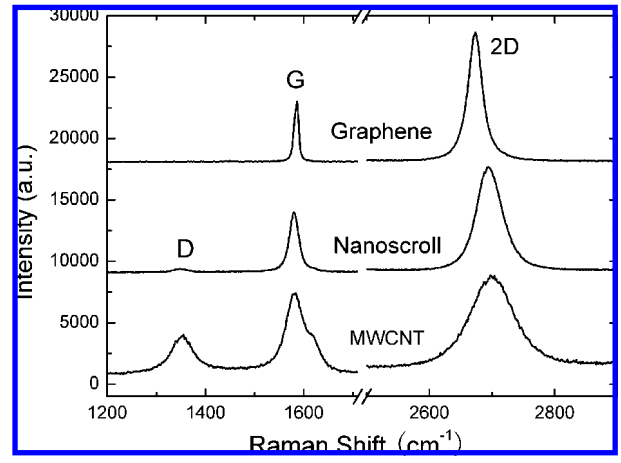

Figure 5. Raman spectra of graphene, CNS, and MWCNT. They are scaled to have a similar height of the G peak at ~1580 cm^{-1}.

The MWCNT-like CNS possesses good morphology and is formed by scrolling a single layer of graphene. Such a well-defined structure facilitates the characterization of its physical properties. More importantly, it is desirable to know what new physical properties the CNS has as compared with CNT and graphene. Since Raman spectra can provide important information about the defects, electronic structure, and phonon dispersion of carbon materials,[24,25] we studied the Raman spectra of the CNS. Figure 5 shows the representative Raman spectra of the graphene monolayer before and after being scrolled, and the referential spectrum of MWCNTs with a diameter of about 15 nm.[26] We have measured many samples, and Table 1 lists the position and full width at half-maximum (FWHM) distribution range of the G peak (~1580 cm^{-1}) and the 2D peak (~2700 cm^{-1}), which are the most intense features in the spectra.

First of all, we can see from Figure 5 that no D peak (~1350 cm^{-1}) is present in our original graphene sample. After it was scrolled, a weak peak appeared at the D peak position. This might be attributed to the few defects induced

Table 1. Comparisons of the G Peak and 2D Peak of Graphene, CNS and MWCNT (cm^{-1})[a]

	position (G)	FWHM (G)	position (2D)	FWHM (2D)
graphene	1583–1590	8–13	2673–2688	26–32
CNS	1580–1582	20–25	2687–2700	35–60
MWCNT	1580–1583	42–45	2699–2703	77–82

[a] A total of 15 CNSs and their graphene counterparts before being scrolled were investigated.

during the fabrication process, or it might be the signal of the graphene edges,[19] especially considering that the laser spot size (1−2 μm) is much larger than the CNS diameter. As to the MWCNT synthesized by chemical vapor deposition, however, we recorded a prominent D peak and another defect-induced peak named D′ (~1620 cm^{-1}). These differences imply that our fabrication process does not deteriorate the quality of the CNS.

It was also noticed that the G peak of monolayer graphene became broader after being scrolled, its FWHM changing from 8−13 to 20−25 cm^{-1} (Table 1). Being accompanied with this broadening was the red shift of its position to about 1580 cm^{-1}, which was almost the same as that of MWCNT (Table 1). While the G peak of monolayer graphene has a wide position distribution (1583−1590 cm^{-1}) because of chemical doping,[27] the G peaks of CNS and MWCNT are almost fixed. Since the G peak originates from the activation of the doubly degenerate zone center E_{2g} phonon mode, it is highly related to the phonon dispersion. Previous work reported that the G peak of graphene red shifts linearly with increasing number of layers,[28] and misoriented stacked layers also showed a red shift of the G peak.[29,30] Here, we argue that it is the same in our case. The interaction of stacked graphene layers might lead to a slight modification of the intra C−C bond in CNS, thus changing the phonon dispersion and moving the G peak. The G peaks of CNS and MWCNT are broader because they are both collections of signals from many stacked graphene layers. It should also be mentioned that, unlike those in small-diameter CNTs,[31] the G peaks of both CNS and MWCNT do not split up into two degenerated modes G+ and G−. This suggests that confinement and curvature do not strongly affect the C−C intra-atomic force constants here, and they can be ignored in our large-diameter tube-like structure.

Finally, we focused on the 2D peak at about 2700 cm^{-1}. As the 2D peak is due to a double-resonant (DR) process, it is closely related to the electronic band structure and the phonon dispersion.[24] The 2D peak is often used to distinguish monolayer graphene (a single sharp 2D peak with FWHM ~30 cm^{-1}) from thicker ones (an asymmetric 2D peak) based on differences in their electronic structures.[19,25,28] Interestingly, although our CNS consists of stacked graphene layers, its 2D band does not show asymmetry as that of a few layers of graphene. On the contrary, there is only a sharp peak that can be well fitted to a single Lorentzian, which is similar to that of monolayer graphene. Theoretical calculations have suggested that the electronic band structure of incommensurately stacked multilayer graphene resembles that of monolayer graphene.[32] Without a defined AB stacking, the weak interlayer interaction is not capable of splitting up the

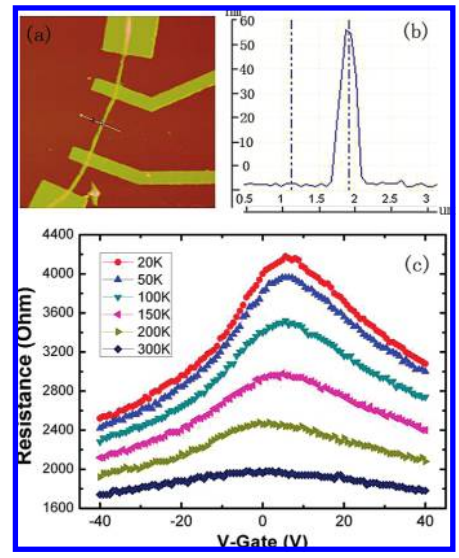

Figure 6. (a) AFM image of a four-point-contacted CNS. (b) AFM height profile across the CNS as indicated by the line in (a). (c) Temperature- and gate-dependent resistance of the CNS.

electronic dispersion curve, so a single peak is preserved in the DR process. To further explain this, we noticed that non-AB stacked graphite (turbostratic graphite) also shows a single 2D peak at 2707 cm^{-1} with about 40 cm^{-1} FWHM,[24] which is very similar to our case. Finally, there is a blue shift and broadening of the 2D peak from graphene to CNS. One possible explanation for this shift is the reduction of Fermi velocity in non-AB staked graphene,[30] and the broadening is presumably due to the overlapping of signals from several graphene layers.

The CNS is easy for device characterization because it has been fabricated on the surface of SiO_2/Si substrate with a defined location. Since there are no previous reports on its electrical properties, it is interesting to probe this issue here. We then fabricated CNS-based field-effect-transistor devices (Figure 6a) by defining source and drain pads on CNS with electron beam lithography (EBL) and carried out temperature- and gate-dependent transport measurements using the four-probe method.

Resistances versus gate-voltage data (Figure 6c) measured in the temperature ranging from 20 to 300 K shows that the resistance of the CNS decreases as the temperature increases. As the gate voltage varies from −40 to 40 V, the resistance slope changes smoothly with a maximum value at the gate voltage around 0−15 V (Figure 6c). This behavior is similar to the transport of a wide graphene nanoribbon, with a ′Λ′-shaped $R-V_g$ curve showing symmetric hole and electron transport.[33,34] However, the $R-V_g$ curve of 2D graphene devices would have a prominent peak ("Dirac Point")[14,35,36] around zero gate voltage rather than the wide and smooth transition observed here. To explain this wide transition, we noticed that the CNS device had a much weaker capacitance coupled with the back gate compared to that of flat graphene, resulting in far fewer carriers under the same gate voltage. The capacitance of the CNS-based device was estimated using $C_{CNS} = (2\pi\varepsilon_0\varepsilon_{r\text{-}eff}L)/(\cosh^{-1}[(R + d)/R])$,[37] with $\varepsilon_{r\text{-}eff} = 2.5$ being the effective dielectric constant of SiO_2, $d =$

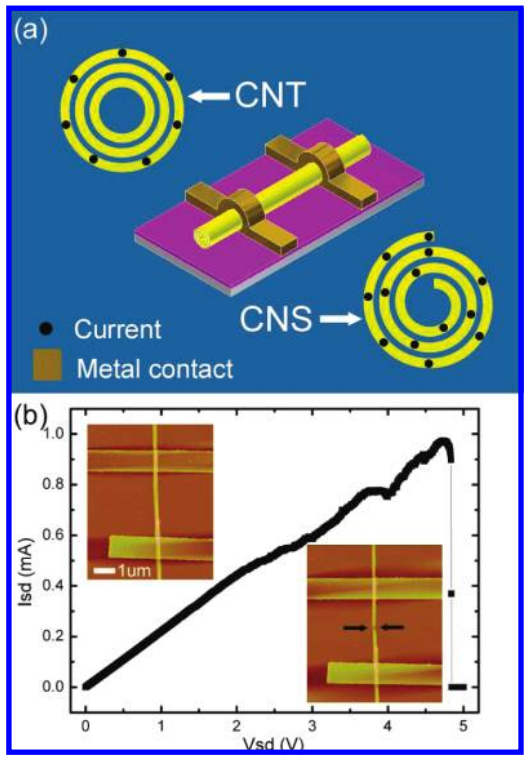

Figure 7. (a) Schematic representations of current conduction at low bias. For CNT, only the outermost shell (which is in direct contact with the metal electrodes) sustains current. For CNS, the current extends to the whole scrolled graphene layer. (b) Current−voltage ($I-V$) curve measured under ambient conditions showing the high-bias electrical characteristics of a CNS about 50 nm in diameter. The breakdown point, which shows the diameter thinning after breakdown, lies midway between the two electrodes.

285 nm is the thickness of SiO_2, $R = 30$ nm (Figure 6b) and $L = 5\ \mu$m are the radius and length of the CNS, respectively. According to the estimation, this capacitance is about one-twentieth of that between flat graphene and SiO_2, suggesting that our measurement only probed the low-carrier-density region around the Dirac Point. In this region, the conductivity of the CNS increased about 2.2 times from 20 to 300 K because of the activation of carriers. Such a strong temperature-dependent conductivity can only be probed in very clean 2D graphene samples,[38,39] like those suspended ones annealed in vacuum.[39] This implies that the CNS device we measured is clean and contains few charge impurities. This is consistent with the aforementioned TEM studies, where the graphene layers were observed to be compactly stacked, and thus no additional room is being provided for impurities in the 0.35 nm spacing.

Finally, we compare the current conduction characteristics of the CNS and MWCNT. For MWCNT, only the outermost shell participates in conduction at low bias (Figure 7a, top left). The inner shells can only couple to the external electrodes through a barrier composed of the outer graphene layers.[40,41] In the CNS, however, current flows through the whole scrolled graphene layer (Figure 7a, bottom right). This difference in conduction should account for the relatively low resistance of the CNS (~kΩ) in the low-bias diffusive transport region. For high-bias transport, the $I-V$ curve of the CNS shows linear behavior as the voltage increases (up to ~2 V) and sublinear behavior (Figure 7b) when the bias is higher. This is quite different from the $I-V$ curve of MWCNT at high bias,[42,43] which shows a current saturation. The final breakdown of the CNS took place at about 5 V with a current density up to 5×10^7 A/cm^2. The breakdown point lay midway between the two electrodes, and the graphene walls nearby were thinned. From its breakdown behavior, we can see that the CNS is of high quality because a large current density can be sustained. Therefore, CNSs might be used for microcircuit interconnects in future circuits.

One more intriguing issue about the CNS is to control its diameter and chirality. The most immediate approach lies in rolling up graphene nanoribbons with various widths and edge directions predefined by EBL from just one graphene sheet. However, this way seems blocked by the contamination induced on graphene surfaces and edges[44,45] during tailoring graphene. Further experiments are needed to clarify the roles and morphologies of the surfaces and edges in the scrolling process.

In summary, we have used IPA solution to roll up monolayer graphene on SiO_2 substrates to form CNSs. On the basis of monitoring the whole scrolling process and elucidating the scrolling mechanism by means of four proposed steps, we have optimized the fabrication to obtain high-quality CNSs. TEM studies show the fabricated CNS exhibits a tubular structure similar to that of MWCNT, the distance between adjacent graphene walls being about 0.35 nm. The Raman spectrum of the CNS confirms that the fabrication process does not bring in significant defects. In addition, it reveals that the electronic structure and phonon dispersion are slightly modified compared with its monolayer graphene counterpart. Lastly, we have fabricated FETs based on CNSs that had been mounted on SiO_2 substrates. Electrical-transport measurements show that the resistance of the CNS decreases strongly with the rise of temperature, indicating that the CNS contains few impurities, which is also consistent with the TEM observations. The current density of the CNS can reach as high as 5×10^7 A/cm^2, which facilitates its application as microcircuit interconnects. Our work is helpful for exploring both the physical properties and applications of CNSs.

Acknowledgment. This work was financially supported by the National Basic Research Program of China (2005CB623606, 2007CB935301), NSFC (10704044, 50825201, 10721404), and Fok Ying Tung Education Foundation (111049). We thank Lihui Zhang and Mo Chen for assistance with EBL fabrication, Lian-mao Peng and Yang Liu for transferring the CNSs to TEM grids, and Qingyu Zhao for help in the video recording.

Supporting Information Available: (1) Fabrication and characterization of monolayer graphene. (2) Process of transferring the CNS to the TEM grid and the TEM study. (3) TEM study of the end of the CNS. (4) Raman spectroscopy study of the CNS. (5) CNS-based devices fabrication and electrical-transport measurements. (6) Video of the scrolling process. This material is available free of charge via the Internet at http://pubs.acs.org.

References

(1) *Carbon Nanotubes: Synthesis, Structure, Properties, and Applications*; Dresselhaus, M. S., Dresselhaus, G., Avouris, Ph., Eds.; Springer: Heidelberg, 2001.
(2) Geim, A. K.; Novoselov, K. S. *Nat. Mater.* **2007**, *6*, 183.
(3) Chen, Y.; Lu, J.; Gao, Z. X. *J. Phys. Chem. C* **2007**, *111*, 1625.
(4) Pan, H.; Feng, Y. P.; Lin, J. Y. *Phys. Rev. B* **2005**, *72*, 085415.
(5) Braga, S. F.; Coluci, V. R.; Legoas, S. B.; Giro, R.; Galvao, D. S.; Baughman, R. H. *Nano Lett.* **2004**, *4*, 881.
(6) Mpourmpakis, G.; Tylianakis, E.; Froudakis, G. E. *Nano Lett.* **2007**, *7*, 1893.
(7) Coluci, V. R.; Braga, S. F.; Baughman, R. H.; Galvao, D. S. *Phys. Rev. B* **2007**, *75*, 125404.
(8) Rurali, R.; Coluci, V. R.; Galvao, D. S. *Phys. Rev. B* **2006**, *74*, 085414.
(9) Bacon, R. *J. Appl. Phys.* **1960**, *31*, 283.
(10) Li, J. L.; Peng, Q. S.; Bai, G. Z.; Jiang, W. *Carbon* **2005**, *43*, 2817.
(11) Viculis, L. M.; Mack, J. J.; Kaner, R. B. *Science* **2003**, *299*, 1361.
(12) Savoskin, M. V.; Mochalin, V. N.; Yaroshenko, A. P.; Lazareva, N. I.; Konstantinova, T. E.; Barsukov, I. V.; Prokofiev, I. G. *Carbon* **2007**, *45*, 2797.
(13) Shioyama, H.; Akita, T. *Carbon* **2003**, *41*, 179.
(14) Novoselov, K. S.; Geim, A. K.; Morozov, S. V.; Jiang, D.; Zhang, Y.; Dubonos, S. V.; Grigorieva, I. V.; Firsov, A. A. *Science* **2004**, *306*, 666.
(15) Novoselov, K. S.; Jiang, D.; Schedin, F.; Booth, T. J.; Khotkevich, V. V.; Morozov, S. V.; Geim, A. K *Proc. Natl. Acad. Sci. U.S.A.* **2005**, *102*, 10451.
(16) Yu, D.; Liu, F. *Nano Lett.* **2007**, *7*, 3046.
(17) Sidorov, A.; Mudd, D.; Sumanasekera, G.; Ouseph, P. J.; Jayanthi, C. S.; Wu, S. Y. *Nanotechnology* **2009**, *20*, 055611.
(18) Blake, P.; Hill, E. W.; Castro Neto, A. H.; Novoselov, K. S.; Jiang, D.; Yang, R.; Booth, T. J.; Geim, A. K. *Appl. Phys. Lett.* **2007**, *91*, 063124.
(19) Ferrari, A. C.; Meyer, J. C.; Scardaci, V.; Casiraghi, C.; Lazzeri, M.; Mauri, F.; Piscanec, S.; Jiang, D.; Novoselov, K. S.; Roth, S.; Geim, A. K. *Phys. Rev. Lett.* **2006**, *97*, 187401.
(20) Watari, M.; Galbraith, J.; Lang, H. P.; Sousa, M.; Hegner, M.; Gerber, C.; Horton, M. A.; McKendry, R. A. *J. Am. Chem. Soc.* **2007**, *129*, 601.
(21) Songmuang, R.; Deneke, Ch.; Schmidt, O. G. *Appl. Phys. Lett.* **2006**, *89*, 223109.
(22) Zang, J.; Huang, M. H.; Liu, F. *Phys. Rev. Lett.* **2007**, *98*, 146102.
(23) Li, X. L. *J. Phys. D: Appl. Phys.* **2008**, *41*, 193001.
(24) Pimenta, M. A.; Dresselhaus, G.; Dresselhaus, M. S.; Cancado, L. G.; Jorio, A.; Saito, R. *Phys. Chem. Chem. Phys.* **2007**, *9*, 1276.
(25) Ferrari, A. C. *Solid State Commun.* **2007**, *143*, 47.
(26) Zhang, X. B.; Jiang, K. L.; Feng, C.; Liu, P.; Zhang, L. N.; Kong, J.; Zhang, T. H.; Li, Q. Q.; Fan, S. S. *Adv. Mater.* **2006**, *18*, 1505.
(27) Casiraghi, C.; Pisana, S.; Novoselov, K. S.; Geim, A. K.; Ferrari, A. C. *Appl. Phys. Lett.* **2007**, *91*, 233108.
(28) Gupta, A.; Chen, G.; Joshi, P.; Tadigadapa, S.; Eklund, P. C. *Nano Lett.* **2006**, *6*, 2667.
(29) Poncharal, P.; Ayari, A.; Michel, T.; Sauvajol, J. L. *Phys. Rev. B* **2008**, *78*, 113407.
(30) Ni, Z. H.; Wang, Y. Y.; Yu, T.; You, Y. M.; Shen, Z. X. *Phys. Rev. B* **2008**, *77*, 235403.
(31) Jorio, A.; Pimenta, M. A.; Souza Filho, A. G.; Saito, R.; Dresselhaus, G.; Dresselhaus, M. S. *New J. Phys.* **2003**, *5*, 139.1.
(32) Latil, S.; Meunier, V.; Henrard, L. *Phys. Rev. B* **2007**, *76*, 201402.
(33) Campos-Delgado, J.; Romo-Herrera, J. M.; Jia, X. T.; Cullen, D. A.; Muramatsu, H.; Kim, Y. A.; Hayashi, T.; Ren, Z. F.; Smith, D. J.; Okuno, Y.; Ohba, T.; Kanoh, H.; Kaneko, K.; Endo, M.; Terrones, H.; Dresselhaus, M. S.; Terrones, M. *Nano Lett.* **2008**, *8*, 2773.
(34) Jiao, L. Y.; Zhang, L.; Wang, X. R.; Diankov, G.; Dai, H. J. *Nature* **2009**, *458*, 877.
(35) Chen, J. H.; Jang, C.; Adam, S.; Fuhrer, M. S.; Williams, E. D.; Ishigami, M. *Nat. Phys.* **2008**, *4*, 377.
(36) Tan, Y. W.; Zhang, Y.; Bolotin, K.; Zhao, Y.; Adam, S.; Hwang, E. H.; Das Sarma, S.; Stormer, H. L.; Kim, P. *Phys. Rev. Lett.* **2007**, *99*, 246803.
(37) Wunnicke, O. *Appl. Phys. Lett.* **2006**, *89*, 083102.
(38) Tan, Y. W.; Zhang, Y.; Stormer, H. L.; Kim, P. *Eur. Phys. J.: Spec. Top.* **2007**, *148*, 15.
(39) Bolotin, K. I.; Sikes, K. J.; Hone, J.; Stormer, H. L.; Kim, P. *Phys. Rev. Lett.* **2008**, *101*, 096802.
(40) Bachtold, A.; Strunk, C.; Salvetat, J. P.; Bonard, J. M.; Forro, L.; Nussbaumer, T.; Schonenberger, C. *Nature* **1999**, *397*, 673.
(41) Huang, J. Y.; Chen, S.; Jo, S. H.; Wang, Z.; Han, D. X.; Chen, G.; Dresselhaus, M. S.; Ren, Z. F. *Phys. Rev. Lett.* **2005**, *94*, 236802.
(42) Collins, P. G.; Hersam, M.; Arnold, M.; Martel, R.; Avouris, P. *Phys. Rev. Lett.* **2001**, *86*, 3128.
(43) Collins, P. G.; Arnold, M. S.; Avouris, P. *Science* **2001**, *292*, 706.
(44) Meyer, J. C.; Geim, A. K.; Katsnelson, M. I.; Novoselov, K. S.; Obergfell, D.; Roth, S.; Girit, C.; Zettl, A. *Solid State Commun.* **2007**, *143*, 101.
(45) Booth, T. J.; Blake, P.; Nair, R. R.; Jiang, D.; Hill, E. W.; Bangert, U.; Bleloch, A.; Gass, M.; Novoselov, K. S.; Katsnelson, M. I.; Geim, A. K. *Nano Lett.* **2008**, *8*, 2442.

NL900677Y